



PERGAMON

Scripta Materialia 45 (2001) 139–144



www.elsevier.com/locate/scriptamat

# Identification of nano-precipitates in a ferritic alloy steel using secondary electron STEM imaging

Jesse G. Nawrocki\*, John N. DuPont, David W. Ackland, and Arnold R. Marder

*Department of Materials Science and Engineering, Lehigh University, 5 East Packer Avenue, Bethlehem, PA 18015, USA*

Received 5 December 2000; accepted 6 March 2001

*Keywords:* Ferritic alloy steel; Scanning transmission electron microscopy; Energy dispersive X-ray analysis

## Introduction

Ferritic alloy steels are used in elevated temperature applications such as in the power generation industry because they possess good high temperature strength and creep resistance. These properties are mainly due to precipitation strengthening of the grain interiors by alloy carbides. Precipitation strengthening is governed by the precipitate size, shape, distribution, and crystallographic orientation with the surrounding matrix. Carbides that provide the strengthening in ferritic alloy steels are typically based on Nb, V, Mo, and W [1–4]. Classical precipitation strengthening of alloys varies as a function of time for a given temperature [5–7]. Initially, clusters of solute atoms form. Eventually, a precipitate forms that is largely coherent with the matrix (i.e., GP zones in an Al alloy) [7]. Precipitates strengthen the matrix because they are obstacles to dislocation movement, which inhibits plastic deformation. Dislocations must either cut through or loop around precipitates. The peak hardness is eventually reached when an ideal particle size and distribution is reached. At this time, the precipitates are partially coherent and semi-coherent.

The precipitates that provide strength in ferritic alloys steels are often carbides that are typically as small as a few nanometers. These precipitates can be difficult to view in a thin foil due to limited atomic number contrast differences between the matrix and precipitate and low visibility of the precipitates in matrices that have high dislocation densities, i.e., martensite or bainite. The precipitates may also be too small to produce diffraction spots used for dark field imaging. In addition, the surrounding matrix can

\* Corresponding author.

E-mail address: jgn0@lehigh.edu (J.G. Nawrocki).

alter the chemical composition and/or diffraction information because the beam will often interact with material around the precipitates. Some of these limitations are overcome by using extraction replicas. This technique allows the precipitates to be unambiguously identified without interference from the matrix. However, small precipitates may still be unresolvable. In addition, many microscopes are incapable of producing a beam size small enough to obtain an EDS spectrum from individual particles. Therefore, it is necessary to use an imaging technique capable of resolving nano-sized precipitates along with a beam size smaller than the precipitates of interest to gain chemical composition information without interference from the surrounding material.

This paper presents the results of a study on the identification of nano-sized carbides present in a ferritic alloy steel. A VG603 FEGSTEM was used to perform secondary electron (SE) STEM imaging of precipitates on carbon extraction replicas. The VG603 allows individual precipitates to be analyzed because the beam size is approximately 1.5 nm, which is smaller than any of the precipitates observed in this study. SE STEM imaging reveals the surface topography of a sample. Therefore, precipitates were easily observed on the carbon film relative to conventional TEM techniques.

## Experimental procedure

The material used was a ferritic alloy steel with the composition shown in Table 1. Many strong carbide-forming elements are present, i.e., V, Nb, W, Mo, and Cr. Carbon extraction replicas were prepared first by polishing to a 0.04  $\mu\text{m}$  finish and etching for approximately 10 s in 2% nital solution. Next, a carbon film was deposited on the sample. The film was then lifted off the sample, along with the precipitates, by applying a current to the sample while immersed in 2% nital solution and capturing pieces of the film on Cu grids.

The ferritic alloy steel samples were simulated coarse-grained heat-affected zones produced using a Gleeble thermo–mechanical simulator. Samples were subjected to a weld thermal simulation representative of an energy input of 2  $\text{kJ mm}^{-1}$ , a peak temperature of 1350°C, and a preheat temperature of 93°C for a 1/2 in. steel plate. Samples were then tempered over a range of temperatures and times and in some cases stress-relaxation tests were done at temperature. A more detailed description of the heat treatments used can be found in Ref. [8].

Carbon extraction replicas were examined using a JEOL 2000FX TEM operating at 200 keV with an  $\text{LaB}_6$  filament, and a VG603 FEGSTEM operating at 300 keV with a probe size of approximately 1.5 nm and a beam current of about 0.5 nA. Both microscopes are equipped with EDS systems.

Table 1  
Chemical composition of the ferritic alloy steel used in this research

Element	C	W	Nb	V	Mo	Cr	Si	Mn	Ni	P	S	B
Wt.%	0.06	1.50	0.05	0.24	0.11	2.52	0.30	0.33	0.07	0.013	0.006	0.0036

## Results and discussion

The identification of second phase precipitates is necessary to understand the properties of a given material. Fig. 1 shows two different micrographs of a carbon extraction replica from similar areas of the same sample. Fig. 1A is a TEM micrograph that shows a prior austenite grain boundary and adjacent matrix area. Many precipitates, identified as Fe-rich  $M_3C$  carbides by comparing EDS spectra with characteristic spectra from the literature [9–11], are readily visible at the prior austenite grain boundary. However, few precipitates are observable within the prior austenite grain interiors, even at higher magnifications. Fig. 1B is a SE STEM micrograph taken at the same magnification as Fig. 1A (note: the boundary shown is not the exact boundary found in Fig. 1A). However, both Fig. 1A and B are representative of typical prior austenite grain boundaries and adjacent regions found in the sample. Many Fe-rich,  $M_3C$  carbides are visible at the prior austenite grain boundary in Fig. 1B similar to Fig. 1A. In addition, many small precipitates are now observable within the prior austenite grains. A higher magnification of the small intragranular precipitates, ranging in size from approximately 5–40 nm, is shown in Fig. 2A. These precipitates were identified as Fe/W-rich carbides (and a small amount of Cr) as shown by the representative EDS spectrum in Fig. 2B, which was taken from an individual particle. The Cu peaks are from the Cu grid and the oxygen peak is contamination on the carbon film or from a passive layer that had formed on the metallographic sample prior to carbon coating. For comparative purposes, an EDS spectrum acquired under similar conditions, but from an area of the carbon extraction replica between precipitates, is shown in Fig. 2C. Shown are peaks for Cu, Si, O, and a very large C peak. This spectrum shows that there

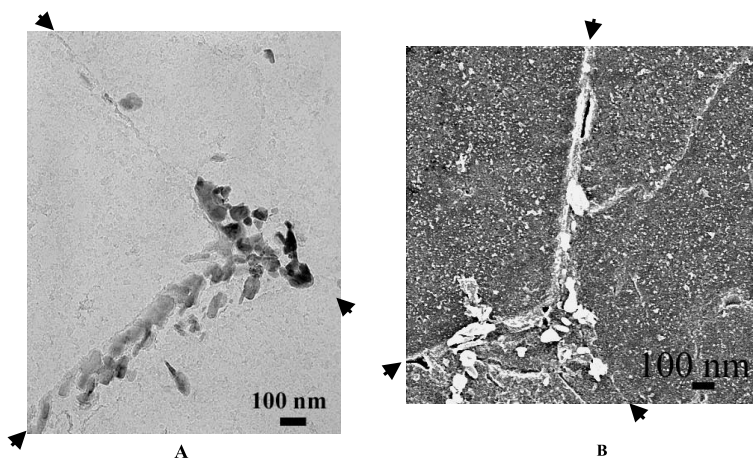


Fig. 1. Representative examples of prior austenite grain boundaries and adjacent intragranular regions of a ferritic alloy steel at the same magnification. Micrographs were taken from a carbon extraction replica using (A) TEM and (B) SE STEM. Prior austenite grain boundaries indicated by arrows. Notice the many small precipitates visible in the intragranular regions of (B).

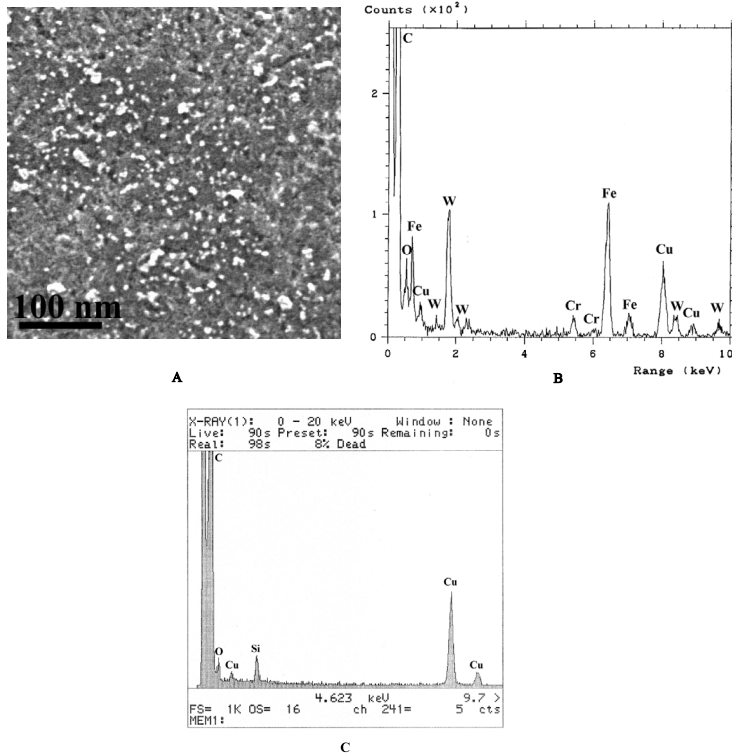


Fig. 2. (A) SE STEM image of a carbon extraction replica of a typical intragranular region of the sample shown in Fig. 1 showing many small precipitates, (B) a representative EDS spectrum of an individual particle from (A) and (C) EDS spectrum from an area of the carbon film between precipitates that was collected under similar conditions as Fig. 2B.

is minimal stray scattering from surrounding particles. Also, this spectrum shows that the O, Cu, and large C peak (due to the relatively thick C-film) are present regardless of the area from which the spectrum was acquired. The silicon K- $\alpha$  peak overlaps with the tungsten L- $\alpha$  peak, but no other tungsten peaks are present in Fig. 2C meaning that the peak is likely Si. This pathological overlap makes the identification of Si very difficult in precipitates containing tungsten. The contribution of stray scattering from precipitates varies according to the distance away from precipitates. In some instances, small peaks of elements present in the precipitates have been identified from spectra taken from areas between particles.

The small precipitates shown in Figs. 1B and 2 are not visible in Fig. 1A. Most conventional TEMs cannot produce a beam small enough to analyze the individual precipitates of Fig. 2 with EDS. The identification of these small precipitates helps to understand certain material properties. Fig. 3 shows two intragranular regions in the same ferritic alloy steel heat-treated under two different conditions. The samples shown in Fig. 3A and B are simulated coarse-grained-heat-affected zones that were tempered at 575°C for 5 h and 725°C for 10 h, respectively. A dense distribution of precipitates, identified as W-rich carbides, is shown in Fig. 3A. The hardness of this sample was 376

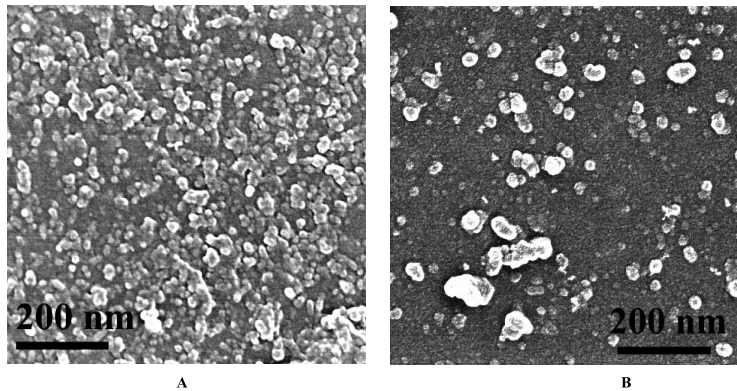


Fig. 3. SE STEM images of intragranular regions of a ferritic alloy steel as a result of two different heat treatments. The samples had hardness values of (A) 376 HKN and (B) 227 HKN. Many small carbides are readily visible.

HKN. Fig. 3B shows an intragranular region of the same material, but different heat treatment, that has a much lower hardness of 227 HKN. The precipitates in Fig. 3B were identified as W/V-rich carbides. The carbides in Fig. 3A and B were not resolvable using conventional TEM methods with the JEOL 2000FX TEM, except of some of the larger carbides. The difference in hardness between the two samples (Fig. 3A and B) is easily understood by comparison of the precipitate morphologies. The higher hardness corresponds to the sample having a relatively denser distribution of carbides and smaller average carbide size. The carbides in Fig. 3B are much coarser than those in Fig. 3A, and qualitatively, the interparticle spacing is greater in Fig. 3B. This makes dislocation movement easier relative to the sample in Fig. 3A where the many precipitates act as barriers to dislocation movement. The differences in hardness could not be easily explained without evidence of these carbides. It should be pointed out, however, that the area fraction shown in Fig. 3A appears to be quite high. This is probably due to the carbon extraction replica procedure. Multiple “layers” of small carbides can be lifted from the material if some larger carbides are also present. The larger the precipitate, the greater the amount of surrounding matrix that must be dissolved before the precipitate can be lifted from the sample. During this time, many smaller precipitates separate from the matrix and attach to the carbon film.

## Conclusions

The carbide precipitation in a ferritic alloy steel was investigated using TEM and STEM methods. Nano-precipitates (5–40 nm) that were unresolvable using conventional TEM methods were easily observed and analyzed using secondary electron imaging with a VG603 FEGSTEM. The small probe size ( $\sim 1.5$  nm) also allowed EDS spectra to be obtained from individual precipitates. This method of analyzing precipitates was extremely helpful in understanding the mechanical properties of this ferritic alloy steel.

**References**

- [1] Davenport, A. T., & Honeycombe, R. W. K. (1975). *Metal Sci* 9, 201.
- [2] Tamaki, K., Suzuki, J., & Li, M. (1993). *Trans Japan Welding Soc* 24, 87.
- [3] Kwon, H., Lee, K. B., Yang, H. R., Lee, J. B., & Kim, Y. S. (1997). *Metall Mater Trans A* 28A, 775.
- [4] Honeycombe, R., & Bhadeshia, H. K. D. H. (1996). *Steels: Microstructure and properties*. New York: Halstead Press.
- [5] Porter, D. A., & Easterling, K. E. (1992). *Phase transformations in metals and alloys*. New York: Chapman and Hall.
- [6] Silcock, J. M., Heal, T. J., & Hardy, H. K. (1953–54). *J Inst Metals* 82, 239.
- [7] Martin, J. W. (1968). *Precipitation Hardening*. Oxford: Pergamon Press.
- [8] Nawrocki J. G. Ph.D. Thesis, Lehigh University, 2000.
- [9] Titchmarsh J. M. (1978). In J. M. Sturgess (Ed.). *Proceedings of the Ninth Inst. Congress on Electron Microscopy* (Vol. 1, pp. 618–619). Toronto: Microscopical Society of Canada.
- [10] Todd, J. A. (1986). *Scripta Metall* 20, 269–274.
- [11] Pilling, J., & Ridley, N. (1982). *Metall Trans A* 13A, 557–563.